Plasma generation and plume expansion for a transmission-mode microlaser ablation plasma thruster

Michael Keidar[a] and Iain D. Boyd
Department of Aerospace Engineering, University of Michigan, Ann Arbor, Michigan 48109

James Luke
New Mexico Institute of Mining and Technology, Albuquerque, New Mexico 87106

Claude Phipps
Photonic Associates, Santa Fe, New Mexico 87505

(Received 12 November 2003; accepted 2 April 2004)

An end-to-end model is presented of the transient plume created by a microlaser ablation plasma thruster. In this article, we describe a model of the plasma generation and expansion for a micro-laser plasma thruster operated in transmission-mode (*T*-mode). The laser ablation and plasma formation processes are modeled using a kinetic ablation model. This procedure provides boundary conditions at the target surface for the plume model that is based on a particle computational approach. The present study considers a 2.5–8 W diode-based laser irradiating a poly-vinyl chloride target for a pulse length of 3–10 ms. Laser beam shape full width at half maximum at the target is about 25×25 μm. The plume simulations reveal many details of the multicomponent plasma expansion. The results are compared with experimentally obtained plume signatures. Generally good agreement between experimental and calculated flux profiles is found. © *2004 American Institute of Physics.* [DOI: 10.1063/1.1753658]

I. INTRODUCTION

There are many future space missions involving science, military, and commercial payloads that require very small thrust levels including very fine attitude control for high resolution Earth imaging and astronomy, and very fine positioning requirements of spacecraft formation flying that is at the core of many interferometry missions. At the same time, many basic components of spacecraft are being miniaturized so that microsatellites and nanosatellites are being designed and built. To satisfy the needs of both the low-thrust missions and the small-scale spacecraft, miniaturized propulsion systems are under development.

Research is being conducted on a variety of microscale spacecraft propulsion systems in response to the needs outlined above. One type of approach involves the scaling down of larger-scale thrusters to the smaller size. However, in most cases, this is only partially successful because the larger thrusters operate in a different physical regime at the small scale for which they are not optimized. For instance: cold-gas thrusters experience significantly larger boundary layers at the microscale in comparison to their large-scale counterparts; Hall thrusters require a significantly stronger magnetic field at the microscale. A separate approach to the design of microscale thrusters attempts to exploit physical mechanisms that work best at the microscale. Several microscale thruster concepts are currently under intensive development, such as micro-pulsed plasma thruster[1] and vacuum arc thruster.[2] Another important example of this type of micropropulsion system is the microlaser-ablation plasma thruster (μ-LPT). Most notably, μ-LPTs have been developed by Phipps *et al.*[3,4] and Gonzalez and Baker.[5] In the present article the μ-LPT design of Ref. 3 is investigated and is described in detail in the following section. In Ref. 5, a *Q*-switched microchip laser, pumped by a cw diode laser, was used to ablate an aluminum target generating thrust in the range of 0.3 to 3 μN with power consumption of about 5 W and pulse frequency in the range of 1 Hz to 10 kHz. The wide dynamic range of thrust levels provided by these devices is one of their most attractive features.

Very recently a similar laser microthruster concept was described by Koizumu *et al.*[6] This thruster utilizes a cylindrical propellant feeding mechanism. They found that introducing carbon additives into the propellant led to a dramatic increase of thruster performance.

A key aspect in the development of any spacecraft propulsion system concerns the assessment of any potential adverse effects that the plume of the thruster may have on the spacecraft. In the case of the plasma plume generated during operation of a μ-LPT, the main integration concerns are (1) plume-induced contamination of the focal lens of the μ-LPT itself (in the case of operating the thruster in the so-called reflection (*R*)-mode]; (2) contamination by the plume of other critical spacecraft components such as solar cells and optical instruments; and (3) erosion of critical spacecraft surfaces due to high energy impact by plume species.

Plume-induced spacecraft damage from a thruster is usually assessed through a combination of experimental and numerical modeling work. Experimental measurement can provide direct data that is relevant to plume effects on the spacecraft. For example, angular profiles of species mass fluxes indicate the potential for contamination, and angular

[a]Electronic mail: keidar@engin.umich.edu

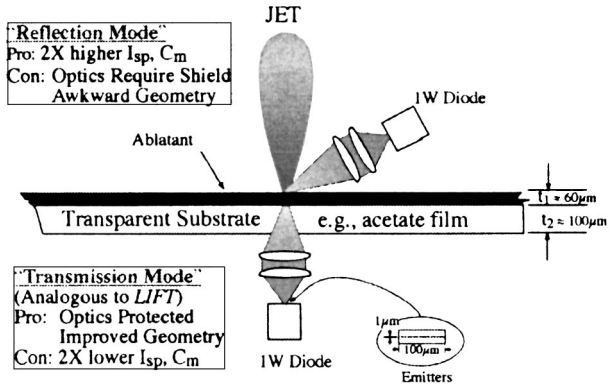

FIG. 1. Schematic diagram of the μ-LPT illustrating the ''reflection'' (R) and ''transmission'' (T) modes.

profiles of ion current density accompanied by ion energy distribution functions indicate the potential for surface erosion. In addition, numerical modeling can also contribute in the assessment of spacecraft integration issues, but only if confidence in a given model can be established.

In the present article, we report on an initial attempt to formulate an end-to-end numerical model of a μ-LPT. The model predicts the products of laser ablation and their properties. These data are then employed as boundary conditions in a detailed model of the plasma plume expansion process. In the following section, a description is first given of the particular μ-LPT considered in the present study. Then, details are provided of the plasma formation and plasma expansion models. Next, results of the models are presented both for the laser ablation and the plasma plume expansion. Finally, the model is assessed by comparison with experimental data.

II. MICROLASER PLASMA THRUSTER

The microlaser-ablation plasma thruster (μ-LPT) developed by Phipps, Luke, and Marquis,[3] Phipps and Luke,[4] Phipps, Luke, and McDuff,[7,8] and Phipps *et al.*[9] uses a 1 to 10 W, high-brightness diode laser irradiating various absorbing material and substrate combinations [e.g., black ink on paper, black poly-vinyl-chloride (PVC) on kapton]. Laser coupling coefficients on the order of 60 μN/W and specific impulses on the order of 500 s with a 1 W laser are achieved. One of the major advantages of the μ-LPT is its large dynamic range of impulse bit that can be varied between 0.4 nN s to 16 μN s by simply increasing the laser pulse duration. In addition, the selection of absorber and substrate materials allows the specific impulse and the laser characteristics to be tailored for specific mission requirements.

As illustrated in Fig. 1, the μ-LPT can be operated in two different modes. In reflection mode (R), the laser is incident on the target and the ablated material ''reflects'' from the surface. This mode has the potential problem of leading to deposition of plume effluent on the laser optics. In transmission mode (T), the laser passes through a transparent substrate film from the back. The substrate is coated on the other side with an absorbing material that ablates material away from the laser. This approach circumvents the problem of optics contamination found with the R mode. However, the dynamic range of impulse bit available in T mode is more restrictive. Coating of laser optics by plume deposition is one of the major lifetime limitations of the μ-LPT in R-mode. Therefore there is a certain preference for development of T-mode operation. In this article, we describe a model of the plasma generation and expansion for a microlaser plasma thruster operated in transmission-mode (T-mode). Preliminary computational results for R-mode μ-LPT were recently presented.[10]

The principle of operation of this device is shown schematically in Fig. 1. A lens focuses the laser diode output onto a 25 μm diameter spot on the transparent side of a fuel tape. The beam heats an absorbing coating to high temperature, producing a miniature ablation jet. The material that is ablated is usually PVC (carbon doped PVC, ranging from 2%–5% C). Typical parameters of operation are power of 2 to 14 W, laser wavelength of 970 nm, and pulse duration of 3–10 ms. The fuel tape thickness is about 185 μm, composed of 125 μm of transparent backing (usually cellulose acetate) and about 60 μm of absorbing coating. Typically Q^* (energy of laser light required to ablate one kilogram of target material) is about 2×10^7 J/kg and the momentum coupling coefficient is about $C_w = 60-100\ \mu$N/W.

Accurate modeling of the μ-LPT plume may provide predictions for the potential spacecraft integration concerns. The goal of this work is to develop models for predicting the end-to-end performance of a μ-LPT, from laser-ablation of a plastic target, to the far-field of the plasma plume. In the following, we first describe a model of the formation of the plasma through laser ablation. Then, a description is provided of the particle model used to simulate the plasma plume expansion of the laser-ablation products.

III. PLASMA GENERATION MODEL

In this section, we describe a model of the plasma layer near the evaporating surface under the effect of the laser beam. It is assumed that most of the laser absorption occurs in this layer. The plasma layer is separated from the surface by a kinetic nonequilibrium (Knudsen) layer that has a thickness of about 20 mean free path.[11,12] It should be noted that an assumption about Knudsen layer thickness does not affect our simulations. Here we use an approach similar to that developed for analyses of Teflon ablation under plasma effects in a pulsed plasma thruster in which the velocity at the edge of the Knudsen layer determines the evaporation rate.[12,13] In general, the velocity at the edge of the Knudsen layer is actually determined by the flow state outside the Knudsen layer.[12] In the case of laser-induced evaporation into vacuum, it is assumed that the ablation is free and therefore the velocity at the edge of the Knudsen layer is equal to the local sound speed.[12]

Solution of the Knudsen layer problem determines the boundary condition for the collision-dominated plasma. Absorption of the laser power leads to thermal evaporation, so that ejected particles obey a Maxwellian velocity distribution at the temperature of the surface T_s.

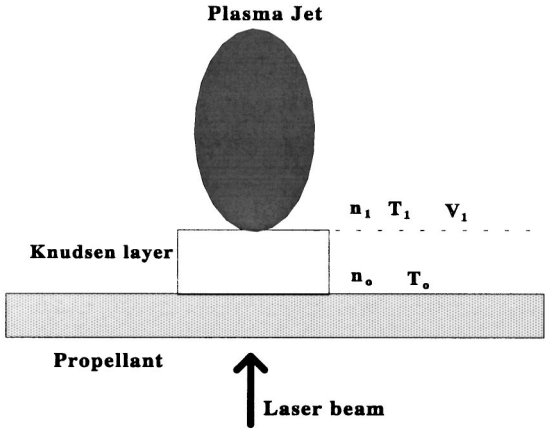

FIG. 2. Schematic of the model for *T*-mode (not to scale).

In this model we assume that local thermodynamic equilibrium (LTE) is established during the laser pulse, since long pulses in the microsecond range are considered. In this case the pulse duration is larger than the typical time for LTE formation. For instance, in a homogeneous transient plasma,[14] complete LTE may be obtained in 0.3 μs for a helium plasma with an electron density of $10^{24}\,\mathrm{m}^{-3}$. An estimation of the characteristic times for ionization and recombination has shown that the ionization and recombination time scales for ground states of C and H are less than the typical time for the laser pulse. In the present case of microsecond range laser pulses, the characteristic times of all collision processes are smaller than the pulse duration and therefore a quasisteady plasma model can be used.

The ablation is modeled in the framework of the approximation based on a kinetic model of material evaporation into discharge plasmas.[13] The model couples two different layers between the surface and the plasma bulk as shown in Fig. 2: (1) a kinetic nonequilibrium layer adjacent to the surface with a thickness of about one mean free path and (2) a collision-dominated layer with thermal and ionization nonequilibrium. The velocity at the edge of the kinetic layer V_1 can be determined from the coupled solution of the hydrodynamic layer and the quasineutral plasma. For known velocity and density at this interface, it is possible to calculate the ablation rate

$$\Gamma = m V_1 N_1 . \tag{1}$$

The system of equations is closed if the equilibrium vapor pressure can be specified that determines parameters (N_0 and T_0) at the ablator surface (unfortunately, the equilibrium vapor pressure of PVC is unknown and therefore we use experimentally obtained parameters to calculate the pressure). The solution of the Knudsen layer problem relates parameters at boundary 1 to the parameters at boundary 0 (Ref. 12). The full self-consistent solution of this problem can be obtained when the ablation is coupled with the plasma plume expansion. In the present work, in order to simplify the problem, we will assume that the plasma accelerates up to the sound speed near boundary 1. In this case the plasma density at the edge of the kinetic layer will be equal to $0.34\,N_0$ and the temperature is $0.67\,T_0$. The flux returned to the surface is equal to 16%–18% of the ablated flux (Refs. 12 and 15). The ablated mass during the pulse can be calculated as $\Delta m = A_s \Gamma \Delta t$, where A_s is the focal spot area and Δt is the pulse duration.

Starting from the above considerations we develop a simplified model of the plasma using the following basic assumptions: (i) the plasma is quasineutral and (ii) the plasma column is in local thermodynamic equilibrium (LTE). The energy balance equation can be written in the form[16]

$$\tfrac{3}{2} n_e V \partial T_p / \partial x = Q_{IB} - Q_{ei} - Q_\lambda , \tag{2}$$

where T_p is the electron temperature in the plasma, n_e is the electron density, $Q_{IB} = \alpha_{IB} I_0 \exp(-\alpha_{IB} x)$ is the power density which is absorbed by electrons via the inverse bremsstrahlung effect, I_0 is the laser power density, α_{IB} is the inverse bremsstrahlung coefficient, Q_{ei} is the rate of energy transfer from electrons to ions, and Q_λ is the rate of energy transfer due to thermal conductivity. Due to the interaction of the laser beam with the plasma, the fraction of the laser power transmitted through the plasma decreases with distance. The temperature inside the PVC ablator can be calculated from the heat transfer equation

$$\partial T / \partial t = a \partial^2 T / \partial x^2 , \tag{3}$$

In order to solve this equation, boundary and initial conditions must be specified[17,18]

$$\begin{aligned} &\lambda \partial T / \partial x (x=0) = q(t) - \Delta H \times \Gamma - C_p (T_s - T_0)\Gamma , \\ &\lambda \partial T / \partial x (x=\infty) = 0, \\ &T(t=0) = T_0 , \end{aligned} \tag{4}$$

where $x=0$ corresponds to the inner dielectric surface, which is in contact with a plasma, ΔH is the ablation heat, Γ is the rate of the ablation per unit area, T_0 is the initial temperature, $q(t)$ is the laser power flux, and T_s is the surface temperature.

Having calculated the plasma density and plasma temperature [Eqs. (1)–(3)] one can calculate the chemical plasma composition considering local thermodynamic equilibrium (LTE) in the way described previously.[17–20] Scanning electron microscope (SEM) analysis of the plume signatures (see below) reveals that the main component in the deposit is carbon. Therefore we start our consideration from the point when we have a gas containing two major components of the propellant products C and H. The Saha equations for each species (C and H) are supplemented by the conservation of nuclei and quasineutrality. The complete system of equations for chemical composition is presented in Refs. 17 and 18.

At the power density level of $10^{10}\,\mathrm{W\,m}^{-2}$ realized in the microlaser plasma thruster,[3] the main mechanism of plasma absorption and therefore electron heating is the inverse bremsstrahlung. The inverse bremsstrahlung coefficient can be calculated as[21,22]

$$\alpha_{IB} = 1.37 \times 10^{-35} \lambda^3 n_e^2 T_e^{-1/2} , \tag{5}$$

where α_{IB} is in cm^{-1}, λ is the laser wavelength in microns, and n_e is the electron density. Under considered condition the inverse bremsstrahlung coefficient varies in the range of

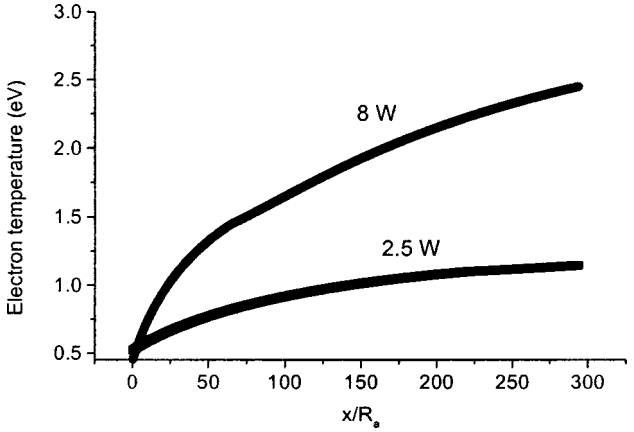

FIG. 3. Electron temperature distribution along the plasma jet originating from the target surface. R_a is the spot radius. Parameters correspond to two cases presented in Table I.

about 1–50 cm^{-1}. As a result the electron temperature increases up to a distance of about few millimeter from the target (as shown in Fig. 3).

An important parameter in laser ablation is the recoil pressure acting on the evaporating surface. The recoil pressure can be calculated as follows:[23]

$$P_r = q_s / L_v (\pi k T_s / 2m)^{0.5}, \tag{6}$$

where q_s is the power density absorbed by the material. On the other hand the recoil pressure can be estimated from experimental data

$$P_r = C_m \times q_s, \tag{7}$$

where C_m is the laser momentum coupling coefficient. Having calculated the ablated mass, one can estimate the parameter Q^* which is the laser energy required to ablate 1 kg. The above system of equations allows the calculation of the plasma temperature and composition during the laser pulse. After the pulse, the plasma cools quickly by radiation and electron conductivity. The solution of the ablation model relies on several assumptions listed above and coefficients, such as the average experimental coupling coefficient. We use these parameters because of the lack of complete data for PVC.

In this article, we consider two specific examples of a μ-LPT operated in *T*-mode for the conditions listed in Table I. In these experiments the laser beam shape full width at half maximum at target was about 25×25 μm. Results are presented for calculation of the plasma generation and expansion under laser ablation of the plastic material used in a microlaser plasma thruster, PVC (poly-vinyl-chloride). Table II contains a list of available fundamental properties of PVC.

TABLE I. μ-LPT conditions.

	1 case (01-10-30a)	2 case (03-2-18c)
Laser power	2.5 W	8 W
Background pressure	1×10^{-2} torr	6.5×10^{-5} torr
Experimental coupling coefficient C_m	226 μN/W	76 μN/W
Q^*	11.4 MJ/kg	10.78 MJ/kg

TABLE II. Physical properties of PVC.

Density	1439 kg/m^3
Thermal conductivity	0.15 W/m K
Specific heat	1.7 kJ/kg K
Heat of vaporization	0.284 MJ/kg

The electron temperature in the plasma generation region is shown in Fig. 3. Two cases (see Table I) are compared. One can see that the case with higher power produces a plasma with a much higher electron temperature. Dependent on the electron temperature, one can expect that the plasma composition will also be different. It should be noted that the calculated electron temperature in the plasma generation region is slightly higher than the measured electron temperature in the laser ablated plume for comparable intensity.[24,25] However plasma plume expansion generally leads to electron cooling and therefore electron temperature in the plume is expected to be smaller than that near the target. The results of the plasma composition calculations are summarized in Table III.

In these calculations we assume that all particles have the same temperature and also the same center-of-mass velocity.[26] It can be noted from Table III that in the second case, the plasma is highly ionized, while in the first case the ionization degree is small. It will be shown below that the plasma composition will affect the plasma plume flowfield.

IV. PLASMA PLUME EXPANSION MODEL

Models for the plumes created by laser ablation have been described previously by Itina, Marine, and Autric[27] and by Franklin and Thareja.[28] In each case, Monte Carlo methods were employed to analyze the effects of a finite back pressure on the plume expansion while the plasma was modeled as a fluid. The focus of these studies was on the use of laser ablation for thin film deposition. The laser spot size was significantly larger in those studies in comparison to that for the μ-LPT considered here.

In the present investigation, a hybrid fluid-particle approach is employed. The heavy-particle products of the laser ablation of PVC (neutral atoms of C and H, and ions C+ and H+) are modeled as particles. Particle collisions are computed using the direct simulation Monte Carlo method

TABLE III. Results of plasma generation modeling.

	Case 1 (01-10-30a)	Case 2 (03-2-18c)
Laser power (W)	2.5	8
Background pressure (torr)	1×10^{-2}	6.5×10^{-5}
Electron temperature (eV)	1.147	2.45
Electron density ($\times10^{23}\,m^{-3}$)	6.836	30.625
C atom density ($\times10^{23}\,m^{-3}$)	10.258	0.2
C ion density ($\times10^{23}\,m^{-3}$)	3.9	10.227
H atom density ($\times10^{23}\,m^{-3}$)	25.4	0.46
H ion density ($\times10^{23}\,m^{-3}$)	2.929	20.398
Velocity (m/s)	4838	7090.37

(DSMC).[29] Both momentum exchange and charge exchange collisions are simulated. Momentum exchange cross sections follow the model of Dalgarno, McDowell, and Williams[30] and the collision dynamics follow the normal DSMC procedures as described in Ref. 29. The implementation of this algorithm for the unsteady plasma plume is described in Ref. 31. The charge exchange processes employ the cross sections proposed by Sakabe and Izawa.[32] No momentum exchange is simulated during charge exchange.

Acceleration of the charged particles in self-consistent electric fields is simulated using the particle-in-cell method (PIC).[33] The plasma potential φ is obtained by assuming charge neutrality to determine the electron number density from the total ion density. By further assuming the electrons are adiabatic, the electron number density n_e is then used in the Boltzmann relation to obtain the plasma potential

$$\varphi - \varphi^* = T^* \frac{\gamma}{\gamma - 1}\left[\left(\frac{n_e}{n^*}\right)^{\gamma - 1} - 1\right], \tag{8}$$

where φ^*, T^*, and n^* are reference values and $\gamma = 5/3$. This approach has been used successfully in our previous work on modeling the plumes of Hall thrusters.[34] In the case of the μ-LPT, the reference point for the Boltzmann relation is taken as the target surface. It is assumed that the potential here is constant.

The two-dimensional (2D) axisymmetric simulation uses a single grid for both the collision and plasma processes. Since charge neutrality is assumed, the PIC cells are not required to be of the order of the Debye length. Instead they are chosen to be small enough to resolve in a reasonable way the gradients in the potential. At the same time, the cells satisfy the DSMC requirement that their size be less than a mean free path. The experimental facility background pressure of the order of 10^{-5}–10^{-2} torr is simulated. In the simulations, this pressure is applied as a fixed background condition with which particles from the thruster can collide. The background pressure gas is assumed to be fully composed of hydrogen atoms at a temperature of 300 K.

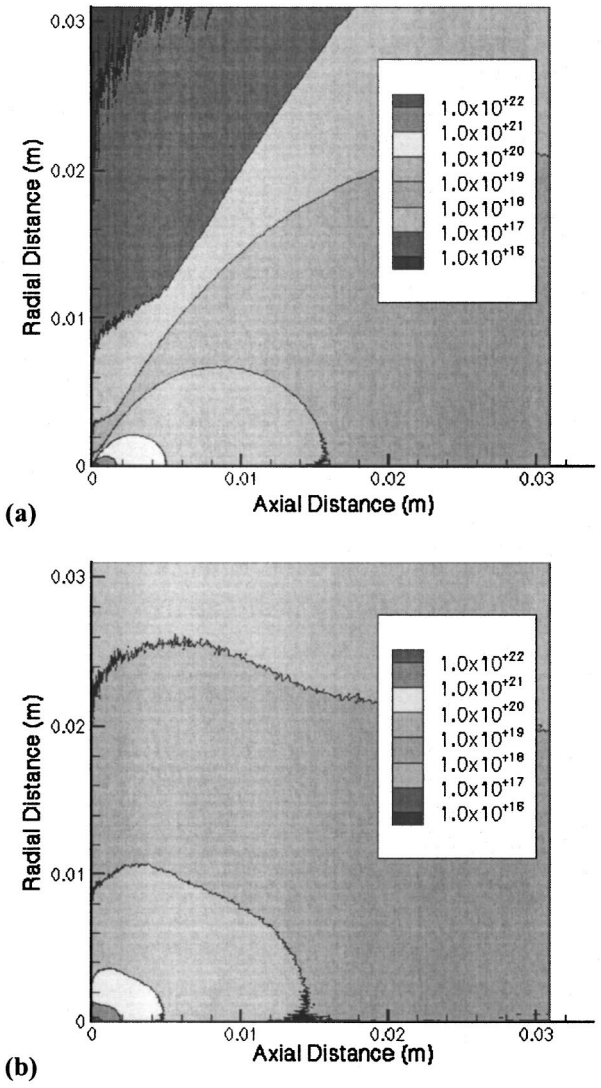

FIG. 4. Contour plots of the plasma number density. Case 2 (Table III). (a) Vacuum and (b) $P = 6.5 \times 10^{-5}$ torr.

V. RESULTS

For simplicity, we consider here a two-component plasma consisting of carbon and hydrogen. The chlorine component of PVC is omitted due to its relatively low abundance. Two examples of a 2.5–8 W diode laser beam focused on a 25 μm radius spot is considered. The pulse duration is 3–10 ms, and the experimentally measured thrust-to-power (coupling coefficient) of about 70–200 μN/W (see Table I) is used in order to estimate the recoil pressure.

The particles injected into the DSMC-PIC simulations are sampled from the equilibrium velocity distribution corresponding to the temperatures and velocities mentioned in Table III. A similar approach has been successfully validated in previous work on simulating the plumes generated in electron beam physical vapor deposition processes.[35,36]

The grid employed in the plume computation contains 300×300 nonuniform rectangular cells. The flow domain extends to about 3 cm in both the axial and radial directions from the center of the ablation spot. A constant time-step of 2×10^{-10} s is employed that is smaller than the smallest collision and plasma time scales (the inverses of the maximum collision and plasma frequencies, respectively).

A steady state is reached after 40 000 iterations and final results are obtained by averaging over a further 50 000 steps. A maximum of more than one million particles is employed in the simulation. Contours of plasma densities are shown in Fig. 4. One can see that background gas pressure strongly affects the plume expansion due to change exchange collisions (CEX) and momentum collisions.

The heavy particle energy distribution at 1 cm and 45° from the spot center are shown in Figs. 5 for higher power case 2 (Tables I, III). Two cases with plume expansion into a vacuum and finite background pressure are shown. One can see that carbon ions and atoms have a higher most probable energy and their distribution is broader than that for the hydrogen ions and atoms. In the case of the finite background pressure, Fig. 5(b), the probability of charge exchange collisions (CEX) increases. In this case a noticeable effect of

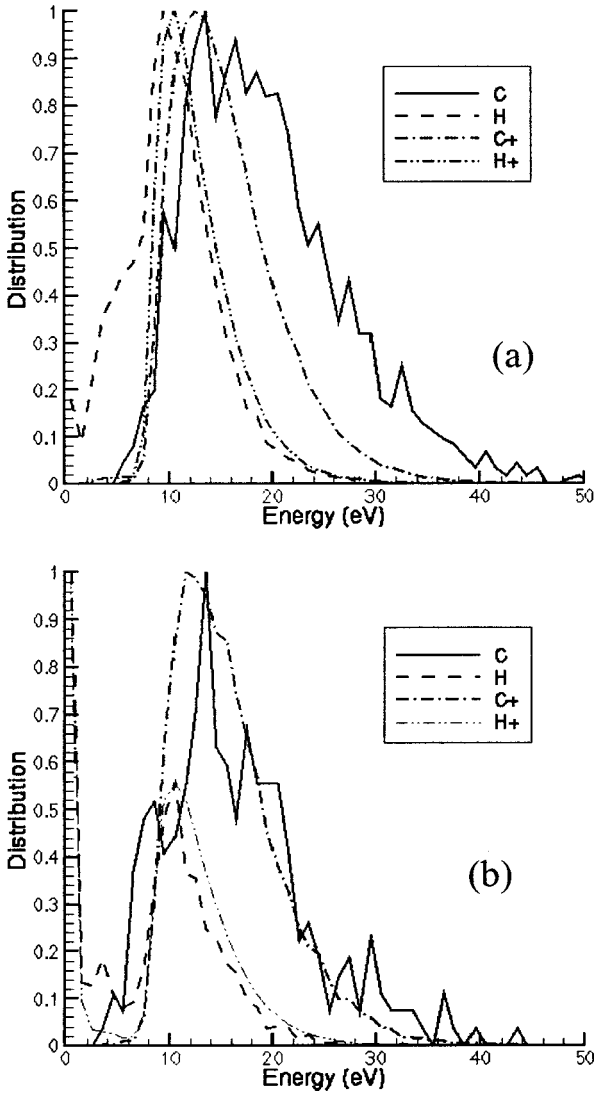

FIG. 5. Heavy particle energy distributions at 1 cm and 45° from the spot center. (a) Vacuum and (b) $P=6.5\times10^{-5}$ torr. Case 2 (Table III).

CEX collisions is obtained in which a significant population of low energy ions is created.

The calculated backflux fraction, which is an important characteristic of the thruster plume for contamination concerns, is shown in Table IV. In all cases the level of backflux is very small (2% at most) although there is a noticeable effect of background pressure.

VI. COMPARISON WITH EXPERIMENT

The distribution of plume deposition on a witness plate was obtained experimentally. The schematic of the experiment is shown in Fig. 6 and plume signatures are shown in Figs. 7. The axes in this figure are labeled in degrees, with 0° corresponding to the direction normal to the tape surface. The shape of the witness plate along the *x*-axis is spherical, while the shape along the *y*-axis is planar. Therefore this leads to dilution of the deposit as shown in Fig. 7(a). In the high-pressure case the plasma plume expansion in the radial direction is limited by collisions with background gas atoms and therefore plasma plume shape is changed [Fig. 7(b)].

TABLE IV. Backflux (ratio of the backward mass flux to the outward mass flux).

	Case 1	Case 2
Vacuum	0.018	0.002556
Background pressure, 6.5×10^{-5} torr	0.0184	0.0107
1×10^{-2} torr	0.0196	–

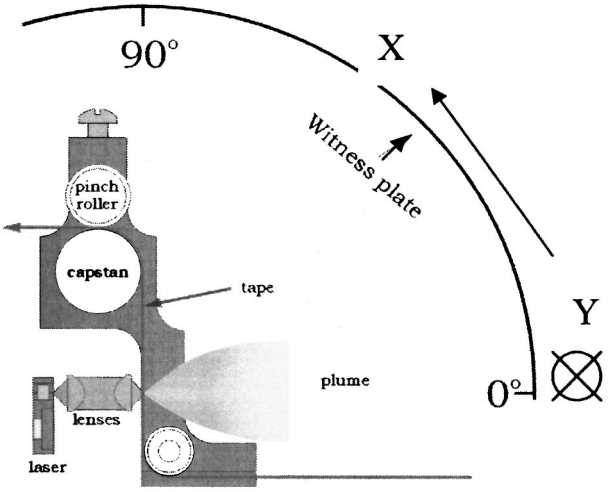

FIG. 6. Schematic of the witness plate deposition experimental setup.

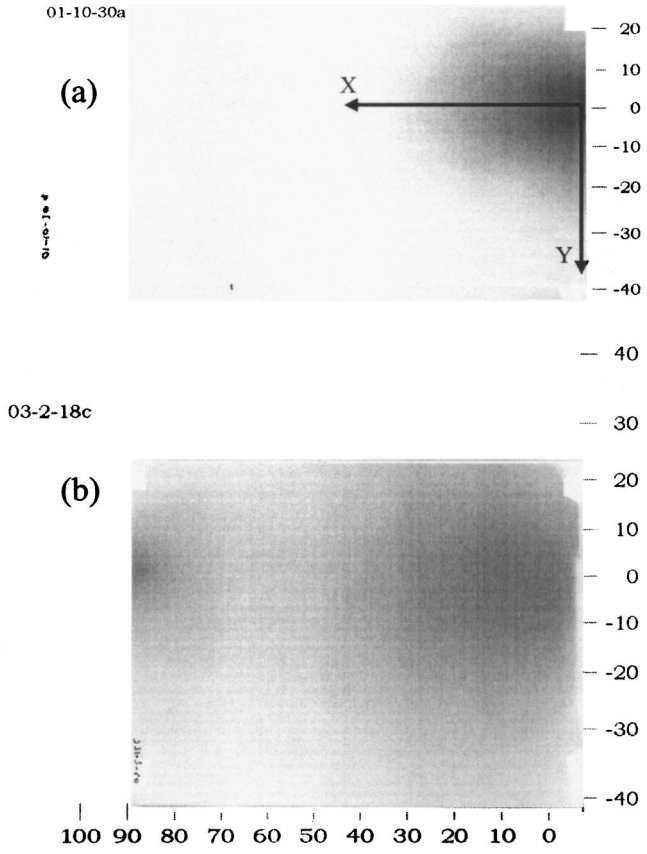

FIG. 7. Experimental plume signature. (a) High pressure case, 1×10^{-2} torr and Experimental plume signature. (b) Low pressure case, 6.5×10^{-5} torr.

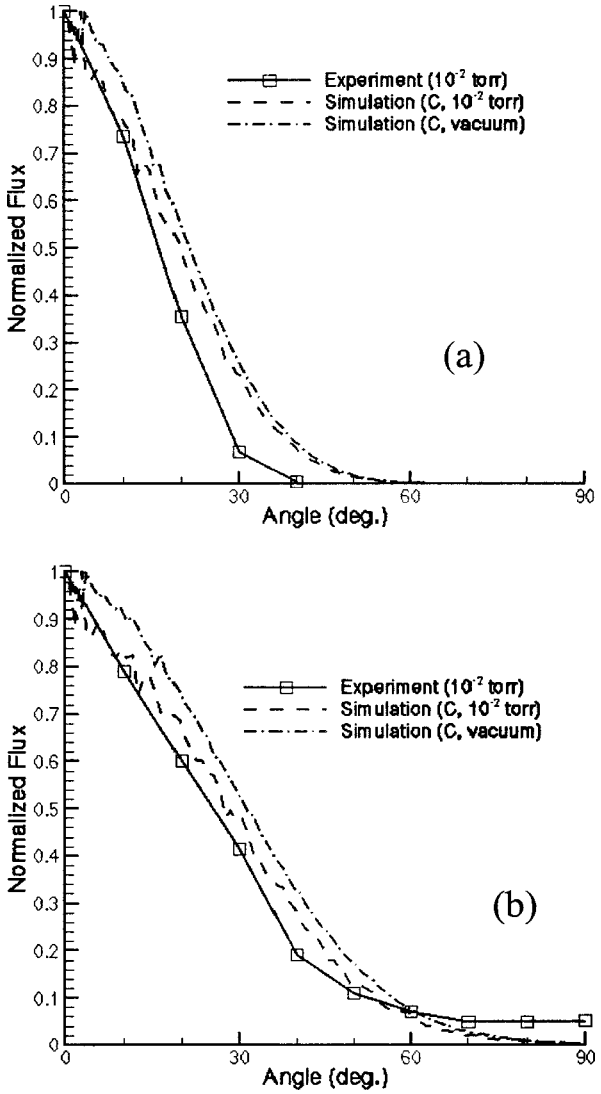

FIG. 8. (a) Normalized flux distribution. High pressure, low power (case 1), *x* direction and (b) Normalized flux distribution. High pressure, low power (case 1), *y* direction.

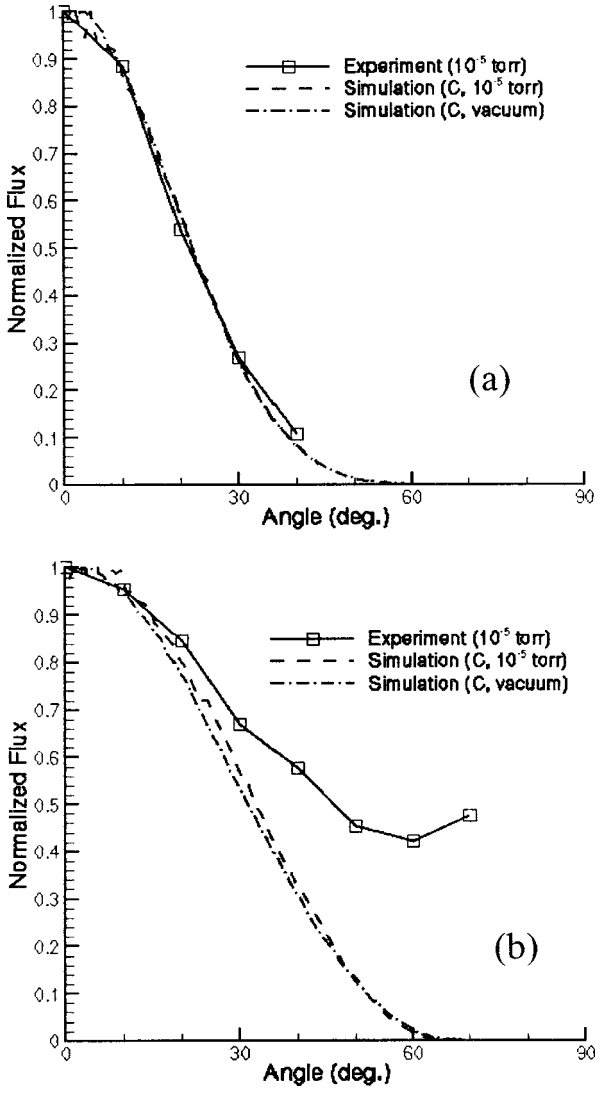

FIG. 9. (a) Normalized flux distribution. Low pressure, high power (case 2), *x* direction and (b) Normalized flux distribution. Low pressure, high power (case 2), *y* direction.

The distance from the laser focus to the cylinder on which the witness plate is rolled is 6 cm. The cylinder is made of metal and mounted to the vacuum chamber so that it is always in the same location. The *x*-axis in the images is the distance around the circumference of the cylinder. The *y*-axis is the distance along the length, and the degree marks are not equally spaced. One can see that in the low-pressure case the plasma plume spreads significantly in comparison with the high-pressure case. The substrate collecting the deposit is the white paper, which is attached to the metal cylinder as shown in Fig. 6. Images were obtained by scanning these papers. These images were analyzed using the software SCION IMAGE.[37] Using this software, the density distribution is quantified (in our case in the *x* and *y* directions across the image, as shown in Figs. 8 and 9).

The normalized flux profiles are shown in Figs. 8 and 9 for all cases (low and high power and low and high pressure, and vacuum). It is assumed that the black deposition material on the witness plate is carbon (this assumption was verified by chemical element analysis of the plume signatures using SEM) and so the simulation results in Figs. 8 and 9 contain the total fluxes of carbon ions and atoms. One can see clear differences in the two deposition signatures and these are due to two effects, namely, the background pressure and operational conditions. The strongest effect of the background pressure can be seen in the higher pressure (case 1) case while in the low pressure case calculations in the vacuum case produces similar results. One can see that the simulations generally predict a narrowing (focusing) of the plume. These results are comparable to previous experimental and theoretical study in the similar background pressure range.[38,39] In this relatively low pressure regime ($<10^{-2}$ torr) the effect of ablated atom collisions with background gas (hydrogen in our case) leads to redistribution of the ablated atoms velocity toward the axial direction. These predictions are confirmed by present experiments as shown in Figs. 7.

It should be noted that the experimental distribution shown in Fig. 9(b) has a second peak, which is not simulated. This peak is due to deflection of the exhaust plume.

This probably occurs due to the fact that when the laser ablates the fuel material and burns into the substrate, the edge of the trench forms a plume-steering surface.[40] One can conclude that overall the comparison of the experimental results and predictions show generally good agreement for the flux profiles in both x and y directions.

VII. CONCLUDING REMARKS

An end-to-end modeling procedure was formulated for predicting the plasma plume structure generated by a micro-laser-ablation plasma thruster operated in T-mode. The model described the laser ablation of a plastic target, the plasma generation at the target surface, and the plasma plume expansion into the far-field. The plasma formation model was based on a fluid approach and assumed equilibrium to calculate the plasma composition. The plasma plume was modeled using a DSMC-PIC approach to include both gas-dynamic and electrostatic acceleration. The plume simulation provided details of the expansion process such as energy distribution functions and deposition profiles. Such data can be used to assess spacecraft contamination issues for the thruster. The plasma plumes were investigated experimentally using depositions on witness plates. These results were compared with model predictions. Generally good agreement between experimental and calculated flux profiles was found.

ACKNOWLEDGMENTS

The work at the University of Michigan was funded by the Air Force Office of Scientific Research under Grant No. F49620-02-1-0084 with Dr. Mitat A. Birkan as the technical monitor. The work at Photonics Associates and the New Mexico University of Mining and Technology was supported by the U.S. Air Force under Contract Nos. F04611-02-M-0025, F49620-00-C-0005, and F49620-98-C-0038.

[1] G. Spanjers, D. R. Bromaghim, Capt. J. Lake, M. Dulligan, D. White, J. H. Schilling, S. S. Bushman, E. L. Antonsen, R. L. Burton, M. Keidar, and I. D. Boyd, *28th AIAA Joint Propulsion Conference*, Indianapolis, IN, USA, July 2002 (American Institute of Aeronautics and Astronautics, Washington, DC, 2002), Paper AIAA-2002-3974.
[2] J. Schein, N. Qi, R. Binder, M. Krishnan, J. K. Ziemer, J. E. Polk, and A. Anders, *27th International Conference on Electric Propulsion*, Pasadena, CA, 2001 (The Electric Rocket Propulsion Society, Worthington, OH, 2001), Paper IEPC-01-238.
[3] C. R. Phipps, J. Luke, and J. Marquis, *36th AIAA/ASME/SAE/ASEE Joint Propulsion Conference*, Huntsville, AL, July 2000 (American Institute of Aeronautics and Astronautics, Washington, DC, 2000), Paper AIAA-2000-3477.
[4] C. Phipps and J. Luke, AIAA J. **40**, 310 (2002).
[5] D. A. Gonzalez and R. P. Baker, *37th AIAA/ASME/SAE/ASEE Joint Propulsion Conference*, July 2001 (American Institute of Aeronautics and Astronautics, Washington, DC, 2001), AIAA Paper 2001-3789.
[6] H. Koizumi, T. Inoue, K. Kojima, K. Mori, K. Komurasaki, and Y. Arakawa, *39th AIAA/ASME/SAE/ASEE Joint Propulsion Conference*, July 2003, Huntsville, AL (American Institute of Aeronautics and Astronautics, Washington, DC, 2003), AIAA Paper 2003-4568.
[7] C. R. Phipps, J. R. Luke, and G. G. McDuff, *27th International Conference on Electric Propulsion*, Pasadena, CA, 2001 (The Electric Rocket Propulsion Society, Worthington, OH, 2001), Paper IEPC-01-220.
[8] C. R. Phipps, J. R. Luke, and G. G. McDuff, *Proceedings 33rd AIAA Plasmadynamics and Lasers Conference*, Maui, 2002 (American Institute of Aeronautics and Astronautics, Washington, DC, 2002), paper AIAA 2002-2152.
[9] C. R. Phipps, J. R. Luke, G. G. McDuff, and T. Lippert, Appl. Phys. A: Solids Surf. **77**, 193 (2003).
[10] I. D. Boyd and M. Keidar, Proc. SPIE **4760**, 852 (2002).
[11] D. Sibold and H. M. Urbassek, Phys. Rev. A **43**, 6722 (1991).
[12] M. Keidar, J. Fan, I. D. Boyd, and I. I. Beilis, J. Appl. Phys. **89**, 3095 (2001).
[13] M. Keidar, I. D. Boyd, and I. I. Beilis, J. Phys. D **34**, 1675 (2001).
[14] H. R. Griem, *Plasma Spectroscopy* (McGraw-Hill, New York, 1964).
[15] D. Sibold and H. M. Urbassek, J. Appl. Phys. **73**, 8544 (1993).
[16] *Principles of Laser plasmas*, edited by G. Bekefi (Wiley, New York, 1976), p. 527.
[17] M. Keidar, I. D. Boyd, and I. I. Beilis, IEEE Trans. Plasma Sci. **28**, 376 (2000).
[18] M. Keidar, I. D. Boyd, and I. I. Beilis, J. Propul. Power **19**, 424 (2003).
[19] P. Kovatya, IEEE Trans. Plasma Sci. **12**, 38 (1984).
[20] C. S. Schmahl and P. J. Turchi, *25th International Conference on Electric Propulsion*, Cleveland, OH (The Electric Rocket Propulsion Society, Worthington, OH, 1997), IEPC 97-124.
[21] Y. Zeldovich and Yu. Raiser, *Physics of Shock Waves and High-Temperature Hydrodynamics Phenomena* (Academic, New York, 1966), p. 259.
[22] J. J. Chang and B. E. Warner, Appl. Phys. Lett. **69**, 473 (1996).
[23] Xi Chen and H. X. Wang, J. Phys. D **34**, 2637 (2001).
[24] B. Toftmann, J. Schou, T. N. Hansen, and J. G. Lunney, Phys. Rev. Lett. **84**, 3998 (2000).
[25] J. M. Hendron, C. M. O. Mahony, T. Morrow, and W. G. Graham, J. Appl. Phys. **81(5)**, 2131 (1997).
[26] R. Kelly and R. W. Dreyfus, Nucl. Instrum. Methods Phys. Res. B **32**, 341 (1988).
[27] T. E. Itina, W. Marine, and M. Autric, J. Appl. Phys. **82(7)**, 3536 (1997).
[28] S. R. Franklin and R. K. Thareja, Appl. Surf. Sci. **177**, 15 (2001).
[29] G. A. Bird, *Molecular Gas Dynamics and the Direct Simulation of Gas Flows* (Clarendon Press, Oxford, 1994).
[30] A. Dalgarno, M. R. C. McDowell, and A. Williams, Proc. R. Soc. London **250**, 411 (1958).
[31] I. D. Boyd, M. Keidar, and W. McKeon, J. Spacecr. Rockets **37**, 399 (2000).
[32] S. Sakabe and Y. Izawa, Phys. Rev. A **45**, 2086 (1992).
[33] C. K. Birdsall and A. B. Langdon, *Plasma Physics via Computer Simulation* (Hilger, London, 1991).
[34] I. D. Boyd and R. A. Dressler, J. Appl. Phys. **92**, 1764 (2002).
[35] J. Balakrisnan, I. D. Boyd, and D. G. Braun, J. Vac. Sci. Technol. A **18**, 907 (2000).
[36] J. Fan, I. D. Boyd, and C. Shelton, J. Vac. Sci. Technol. A **18**, 2937 (2000).
[37] www.scioncorp.com
[38] D. J. Lichtenwalner, O. Auciello, R. Dat, and A. I. Kingon, J. Appl. Phys. **74**, 7497 (1993).
[39] J. C. S. Kools, J. Appl. Phys. **74**, 6401 (1993).
[40] J. R. Luke, C. R. Phipps, and G. G. McDuff, Proc. SPIE **4760**, 843 (2002).